Mon. Not. R. Astron. Soc. **000**, 000–000 (0000) Printed 4 August 2010 (MN LaTeX style file v2.2)

arXiv:1008.0582v1 [astro-ph.SR] 3 Aug 2010

First *Kepler* results on compact pulsators III: Subdwarf B stars with V1093 Her and hybrid (DW Lyn) type pulsations.

M. D. Reed,[1]⋆ S. D. Kawaler,[2] R. H. Østensen,[3] S. Bloemen,[3], A. Baran,[2,4] J. H. Telting,[5] R. Silvotti,[6] S. Charpinet,[7] A. C. Quint,[1] G. Handler,[8] R. L. Gilliland,[9] W. J. Borucki,[10] D. G. Koch,[10] H. Kjeldsen,[11] and J. Christensen-Dalsgaard[11]

[1]*Department of Physics, Astronomy and Materials Science, Missouri State University, 901 S. National, Springfield, MO 65897, USA*

[2]*Department of Physics and Astronomy, Iowa State University, Ames, IA 50011, USA*

[3]*Instituut voor Sterrenkunde, Katholieke Universiteit Leuven, Celestijnenlaan 200 D, 3001 Leuven, Belgium*

[4]*Krakow Pedagogical University, ul. Podchorążych 2,30-084 Kraków, Poland*

[5]*Nordic Optical Telescope, 38700 Santa Cruz de La Palma, Spain*

[6]*INAF-Osservatorio Astronomico di Torino, Strada dell'Osservatorio 20, 10025 Pino Torinese, Italy*

[7]*Laboratoire d'Astrophysique de Toulouse-Tarbes, Université de Toulouse, CNRS, 14 Av. E. Belin, 31400 Toulouse, France*

[8]*Institut für Astronomie, Universität Wien, Türkenschanzstrasse 17, 1180 Wien, Austria*

[9] *Space Telescope Science Institute, 3700 San Martin Drive, Baltimore, MD 21218, USA*

[10]*NASA Ames Research Center, MS 244-30, Moffett Field, CA 94035, USA*

[11]*Department of Physics, and Astronomy, Building 1520, Aarhus University, 8000 Aarhus C, Denmark*

Accepted Received

ABSTRACT

We present the discovery of nonradial pulsations in five hot subdwarf B (sdB) stars based on 27 days of nearly continuous time-series photometry using the *Kepler spacecraft*. We find that *every* sdB star cooler than $\approx 27\,500\,\mathrm{K}$ that Kepler has observed (seven so far) is a long-period pulsator of the V1093 Her (PG 1716) class or a hybrid star with both short and long periods. The apparently non-binary long-period and hybrid pulsators are described here. The V1093 Her periods range from one to 4.5 h and are associated with $g-$mode pulsations. Three stars also exhibit short periods indicative of $p-$modes with periods of 2 to 5 m and in addition, these stars exhibit periodicities between both classes from 15 to 45 m. We detect the coolest and longest-period V1093 Her-type pulsator to date, KIC010670103 ($T_{\mathrm{eff}} \approx 20\,900\,\mathrm{K}$, $P_{\mathrm{max}} \approx 4.5$ h) as well as a suspected hybrid pulsator, KIC002697388 which is extremely cool ($T_{\mathrm{eff}} \approx 23\,900\,\mathrm{K}$) and for the first time hybrid pulsators which have larger $g-$mode amplitudes than $p-$mode ones. All of these pulsators are quite rich with many frequencies and we are able to apply asymptotic relationships to associate periodicities with modes for KIC010670103. *Kepler* data are particularly well-suited for these studies as they are long-duration, extremely high duty cycle observations with well-behaved noise properties.

Key words:
Stars: oscillations – stars: variables – Stars: subdwarfs

1 INTRODUCTION

Subdwarf B (sdB) stars are horizontal-branch stars with masses near $0.5\mathrm{M}_{\odot}$, thin ($< 10^{-2}\mathrm{M}_{\odot}$) hydrogen shells, and temperatures from $22\,000$ to $40\,000$ K (Heber 1984; Saffer et al. 1994). Asteroseismology of pulsating sdB stars can potentially probe the interior structure and provide estimates of total mass, shell mass, luminosity, helium fusion cross sections, and coefficients for radiative levitation and gravitational diffusion. To apply the tools of asteroseismology, however, it is necessary to resolve the pulsation frequencies. This usually requires extensive photometric campaigns, preferably at several sites spaced in longitude to reduce diurnal aliasing. *Kepler's* space-based vantage point provides data that are well suited for asteroseismic studies as they are practically continuous, evenly sampled, and uniform.

Pulsating sdB stars have two classes which seem to form a continuous sequence in temperature. The short-period pulsators were discovered in 1997 (Kilkenny et al. 1997) and were named EC 14026 stars after that prototype. Their official designation is V361 Hya stars, but they are commonly referred to as sdBV stars. Their periods are typically two to three minutes, but can be as long as 5 minutes with amplitudes typically near 1% of their mean brightness (see Reed et al. 2007b, for a review of 23 pulsators). These are $p-$mode pulsators with driving likely produced by an iron-enhanced κ-mechanism (Charpinet et al. 1996, 2001). Recent work suggests that about 10% of hot sdB stars belong to this class (Østensen et al. 2010a,b). Long-period pulsators were discovered in 2003 (Green et al. 2003) and referred to as PG 1716 stars, after that prototype and officially designated as V1093 Her stars. Their periods range from 45 m to 2 h with amplitudes typically $<$0.1% though amplitudes up to 0.5% of their mean brightness have been observed. These are $g-$mode pulsators with driving also caused by the iron κ-mechanism (Fontaine et al. 2006) and they are cooler then the V361 Hya stars, though there may be some overlap. Hybrid

---

⋆ E-mail:MikeReed@missouristate.edu

sdBV stars were first discovered in 2006 with the prototype being DW Lyn (Schuh et al. 2006). They all have temperatures at the V361 Hya – V1093 Her border, and prior to these *Kepler* data, 4 were known (Schuh et al. 2006; Baran et al. 2005; Lutz et al. 2009; Baran et al. 2010). An interesting property of the hybrids is that they have some uncharacteristically high-amplitude frequencies for both $p-$ and $g-$mode pulsations. As an example, in Balloon 090100001 (hereafter BA09) the highest amplitude $p-$mode is at 2807.5μHz with a V-band amplitude of 53.34 mma and the highest amplitude $g-$mode is at 325.6μHz with an ampitude of 2.19 mma (Baran et al. 2010). Both of these amplitudes are a factor of ten higher then average non-hybrid stars. For the hybrids, the highest-amplitude $p-$ and $g-$mode pairs of amplitudes are $21.7, 3.7$; $53.34, 2.19$ (V-band); $6.6, 1.5$; and $18.8, 2.2$ mma (milli-modulation amplitudes) for HS 0702+6043, BA09, HS2201+2610 and RATJ0455+1305, respectively (Schuh et al. 2006; Baran et al. 2005; Lutz et al. 2009; Baran et al. 2010). BA09, which is the best studied of these stars, also shows a series of low-amplitude modes that nearly span the gap between the $g-$ and $p-$mode ranges (Baran et al. 2009). A broad review of sdB stars can be found in Heber (2009).

In this paper we examine the apparently non-binary $g-$mode sdB pulsators discovered during the *Kepler Mission* data released in December 2009. These have *Kepler Input Catalog* (KIC) numbers of 007664467 and 010670103 for the V1093 Her-type and 002697388 (identified in the Sloan SEGUE extension survey as SDSS J190907.14+375614.2, Yanny et al. 2009), 003527751 (also in the Sloan SEGUE survey as SDSS J190337.02+383612.5, Yanny et al. 2009) and 005807616 (previously identified as KPD 1943+4058, Downes 1986, and hereafter KPD 1943) for the hybrid stars. Their *Kepler* system magnitudes are listed as 16.45, 16.53, 15.02 15.39, and 14.86, respectively. Spectroscopic properties of these stars are published in Østensen et al. (2010b, hereafter, Paper I) using metal line blanketed LTE models of solar metalicity. They are $T_{\rm eff}$ $\log g$ of $\approx 26\,800\,$K, 5.17 for KIC007664467; $\approx 20\,900\,$K, 5.11 for KIC010670103; $\approx 23\,900\,$K, 5.32 for KIC002697388; $\approx 27\,600\,$K, 5.28 for KIC003527751; and $\approx 27\,100\,$K, 5.51 for KPD 1943. KPD 1943 was already suspected to be a long-period pulsator from pre-*Kepler* observations (Silvotti et al. 2009) and we confirm those observations. The binary $g-$mode sdB pulsators appear in Kawaler et al. (2010b, Paper V).

The *Kepler Mission* science goals, mission design, and overall performance are reviewed by Borucki et al. (2010) and Koch et al. (2010). Asteroseismology for *Kepler* is being conducted through the *Kepler Asteroseismic Science Consortium* (KASC; Gilliland et al. 2010a). These data were obtained as part of the survey mode, where short-cadence targets are rotated every month during the first year (Gilliland et al. 2010a,b). The striking advantage to *Kepler* data are the many improvements over ground-based data, particularly for $g-$mode-regime variability. From the ground, one can only observe a few pulsation cycles during night time hours and if multisite observations are obtained, then differing instrument sensitivities become an issue, and because of weather, gaps will inevitably appear in the data. Additionally, ground-based observations have to contend with atmospheric issues, such as transparency that can often change on the timescales near that of the intrinsic variability for $g-$mode sdBV stars. As such, *Kepler* data are really optimal for these types of pulsators in that nearly gap-free data were obtained at a roughly constant cadence and with no atmospheric issues. This advantage allows us to detect many more pulsation frequencies than Earth-bound telescopes can obtain, even with significant multisite effort.

Other *Kepler* papers in this sequence on sdBV stars include Paper I (Østensen et al. 2010b), which summarizes target selection and spectroscopic properties; Paper II (Kawaler et al. 2010a), which examines the first V361 Hya variable; Paper IV (Van Grootel et al. 2010) which provides a model fit to KPD 1943; and Paper V (Kawaler et al. 2010b), which discusses V1093 Her stars in close binaries.

2 OBSERVATIONS

This paper describes data obtained by the *Kepler Mission* during 2009. The data released to the KASC compact stars working group (WG11) are short cadence data with an average integration time of 58.8 s. Data on all five pulsators described in this paper were obtained during Q2.3 (the third month of the second quarter) over a 27 d span between BJD 2455064 and 2455091 (20 August - 16 September, 2009) and released to the KASC on 31 December, 2009. The temporal frequency resolution is 0.43μHz for these data and during these ≈ 27 days of observations, a total of 45,210 science images were scheduled. However, because of a 22.5 h safing event and other small glitches, including loss of fine guidance, $\approx 3\,700$ images were either not obtained or were contaminated in some way. These images were not used in our analysis. It has also been found that the long cadence reading of the CCDs affects the short cadence data by creating artefact peaks at $n \cdot 566.391\,\mu$Hz. For most of these data, variation frequencies are short of $566.391\,\mu$Hz and for the short periodicities we were careful to avoid these artefacts. Another *Kepler* processing step is a contamination-correction, which describes what fraction of the flux is from nearby stars in the 4 arcsecond aperture. These contamination fractions are 87.9, 45.0, 14.9, 8.1, and 33.2% for KIC007664467, KIC010670103, KIC002697388, KIC003527751, and KPD 1943 respectively. Some of these fractions are so large (most of the flux for KIC007664467 is attributed to nearby stars), that the actual amplitudes (measured as deviations from the mean flux) may be significantly different, though relative amplitudes within each star would not be affected. For this paper, we used uncorrected flux as suggested in Paper I because we found the photometric temperatures in the *Kepler* Input Catalogue to be cooler than those from spectroscopy. Until the contamination process is sorted out, it is safer to use the raw fluxes, and a correction can be applied later to determine the intrinsic amplitudes.

Kepler data on these stars were provided with times in barycentric corrected Julian days, and fluxes which are shown in Figs. 1 and 2. Note the gap during the data that corresponds to a safing event during day 22. We normalized the flux and amplitudes are given as parts-per-thousand (or milli-modulation amplitude, mma), with 10 mma corresponding to 1.0%.

Note that at the time of this writing the pipeline for reducing *Kepler* short cadence data is still being fine-tuned and tested. As a result, it is possible that some frequencies and amplitudes could be affected by the current *Kepler* reduction pipeline with differing results in subsequent data releases as the process is improved.

3 ANALYSES

Our analysis proceeded in a straightforward way; we calculated a temporal spectrum (also known as a Fourier transform; FT) which was used for initial estimates of frequencies and amplitudes. We simultaneously fitted and prewhitened the data using non-linear least-squares (NLLS) software beginning with the highest amplitude frequency until we reached the $4\,\sigma$ detection limit or unresolved frequencies, which we were unable to fit.

We determined 4σ detection limits using apparently variation-free frequency regions surrounding those with periodicities. For KIC007664467 we used regions bracketing the variations at 40-80, and 300-500 μHz which gave a detection limit of 0.31 mma. For KIC010670103 the bracketing regions used were 20-50 and 205-235, which gave a limit of 0.24 mma. For KIC002697388, we chose regions that appeared pulsation-free between 50-75, and 350-450 μHz for the low-frequency regime with a limit of ranging from 0.23 mma on the long side to 0.13 mma on the short side and 2000-3700 μHz for the high-frequency regime with a detection limit of 0.11 mma. For KIC003527751 we used low-frequency regions of 20-80 and 300-360 μHz with resulting limits of 0.11 and 0.07 mma, respectively, and 2000-3600μHz for a high-frequency range with a limit of 0.07 mma. The regions used to calculate the noise were: 20-75, 450-500 and 2000-3400 μHz

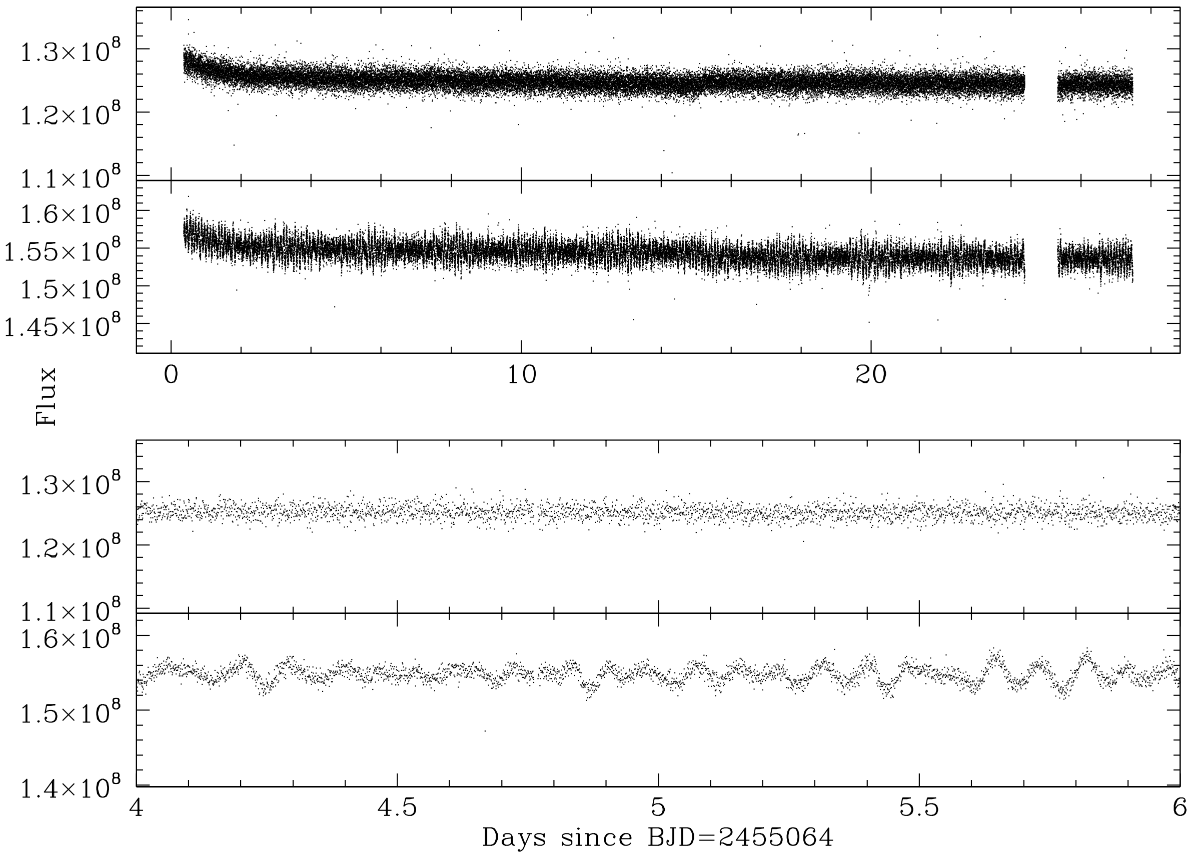

Figure 1. Light curves of the V1093 Her variables KIC007664467 (top) and KIC010670103 (bottom). The horizontal axis is in days, and the vertical axis shows the raw flux (in counts per second). The upper panels show the complete light curves, while the lower ones show shorter segments.

for KPD1943 which produced a long-period detection limit of 0.09 mma and a short-period limit of 0.07 mma.

In the tables, we include a signal-to-noise (S/N) measurement for each frequency, measured in standard deviations with the detection limit shown as a solid (blue) horizontal line in the figures. Also in the figures, we include another more conservative estimate which uses the mean of the peaks in the temporal spectra, rather than the mean of the entire spectra shown as a red line.

3.1 V1093 Her variables

For the two V1093 Her variables, the pulsation amplitudes are readily seen in the temporal spectra. Because of their large contamination fractions, it is expected that compared to “normal” V1093 Her variables, these all have some high-amplitude frequencies. Additionally, they are all clearly multimode pulsators with many peaks in their temporal spectra. NLLS fitting and prewhitening was a pretty straightforward exercise, except where noted below for individual stars.

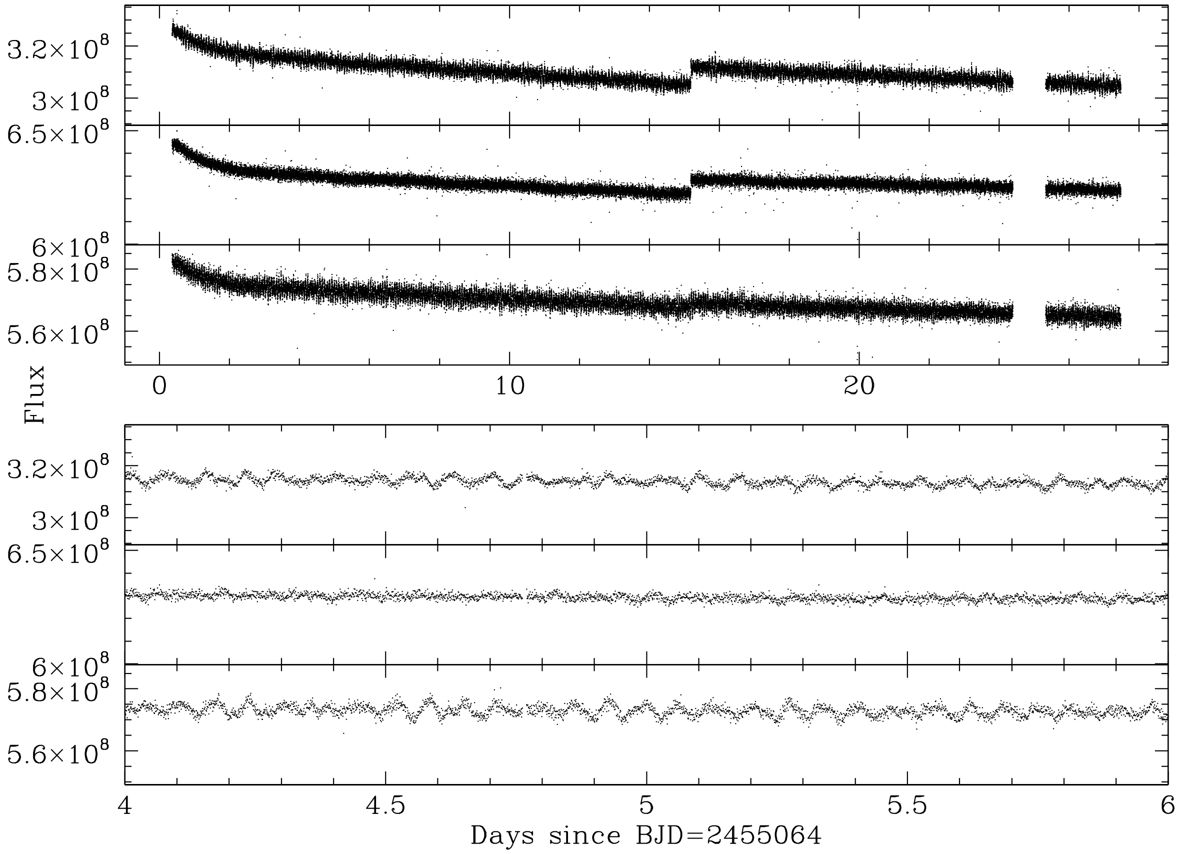

Figure 2. Same as Fig.1 for the hybrid variables KIC002697388 (top), KIC003527751 (middle), and KPD 1943 (bottom).

3.1.1 KIC007664467

KIC007664467 ($K_p = 16.45$, $T_{\rm eff} \approx 26\,800 \pm 500\,{\rm K}$, $\log g = 5.17 \pm 0.08$; Paper I) has the lowest S/N peaks of all the stars in this paper, resulting in the fewest frequencies detected (six with confidence, another one less-so at a S/N of 3.76). These are listed in Table 1 along with their amplitudes and periods and indicated in Fig. 3 with blue and magenta arrows, respectively. Prewhitening effectively removes all power above the detection limit and clearly there are other peaks below the detection limit which are likely produced by stellar variations. With improved data, which we anticipate obtaining in the future with *Kepler*, we should be able to ascertain if those peaks are intrinsic to the star or noise.

3.1.2 KIC010670103

We detected a total of 28 frequencies for KIC010670103 ($K_p = 16.53$, $T_{\rm eff} \approx 20\,900{\pm}300\,{\rm K}$, $\log g = 5.11 \pm 0.04$; Paper I), with lots of power still remaining, but just below the detection limit. These

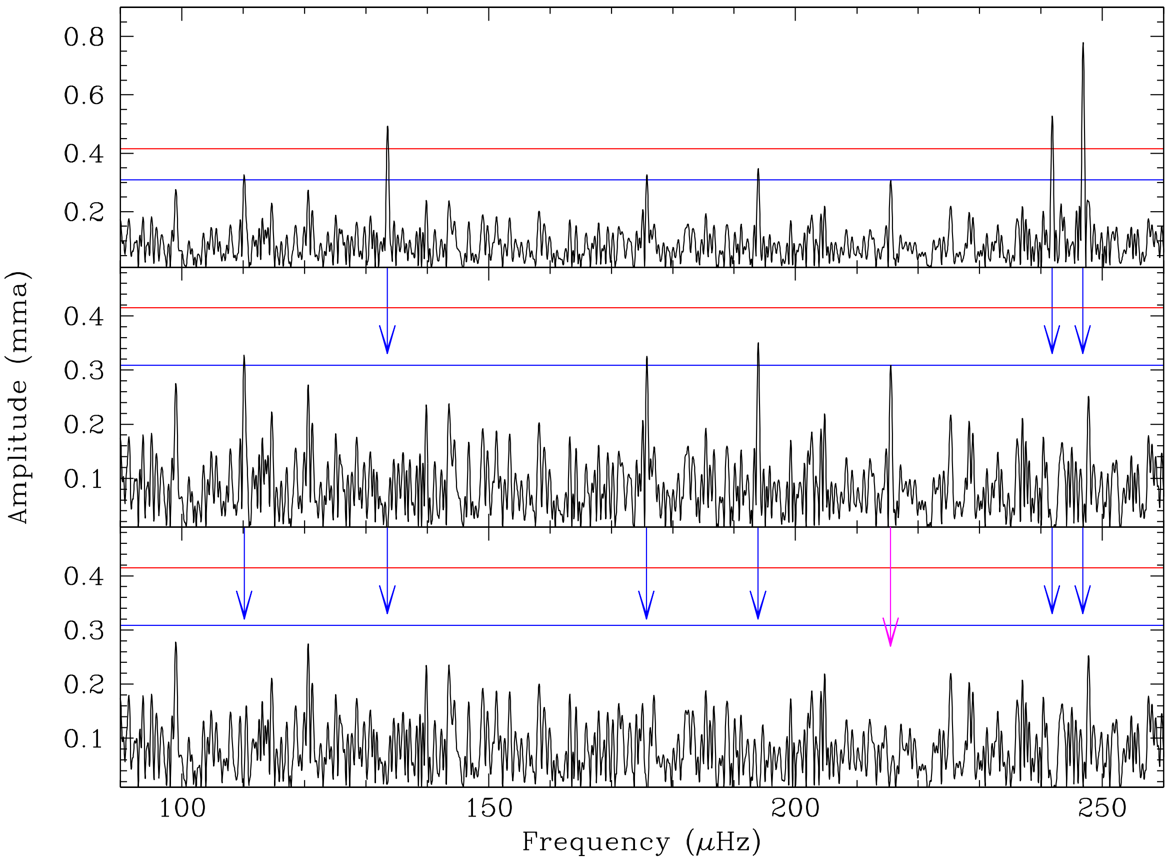

Figure 3. Temporal spectrum and prewhitening sequence for KIC007664467. The solid (blue) horizontal line is the 4σ detection limit, the dashed (red) horizontal line is the peak 4σ detection limit, and arrows indicate prewhitened frequencies.

Table 1. Frequencies, periods, amplitudes, and S/N for KIC007664467. Frequencies below the 4σ detection limit are listed as *suggested*.

ID	Frequency (μHz)	Period (s)	Amplitude (mma)	S/N σ
f1	110.179 (0.045)	9076.175 (3.719)	0.317 (0.060)	4.1
f2	133.551 (0.030)	7487.792 (1.683)	0.478 (0.060)	6.2
f3	175.789 (0.044)	5688.625 (1.423)	0.326 (0.060)	4.2
f4	193.932 (0.041)	5156.458 (1.081)	0.352 (0.060)	4.6
f5	241.826 (0.028)	4135.197 (0.486)	0.505 (0.060)	6.5
f6	246.872 (0.019)	4050.680 (0.308)	0.765 (0.060)	9.9
	Suggested frequency			
s7	215.491 (0.050)	4640.562 (1.081)	0.285 (0.060)	3.7

frequencies are listed in Table 2 along with their amplitudes and periods and indicated in Fig. 4 by arrows.

As indicated in Table 2, several of the frequencies appear as possible combinations or differences of other frequencies, some with multiple combinations which could interact in very complex ways. As model frequency densities are quite high (see Paper IV), it is likely these are chance alignments and so are mentioned solely for completeness. A far more compelling interpretation of

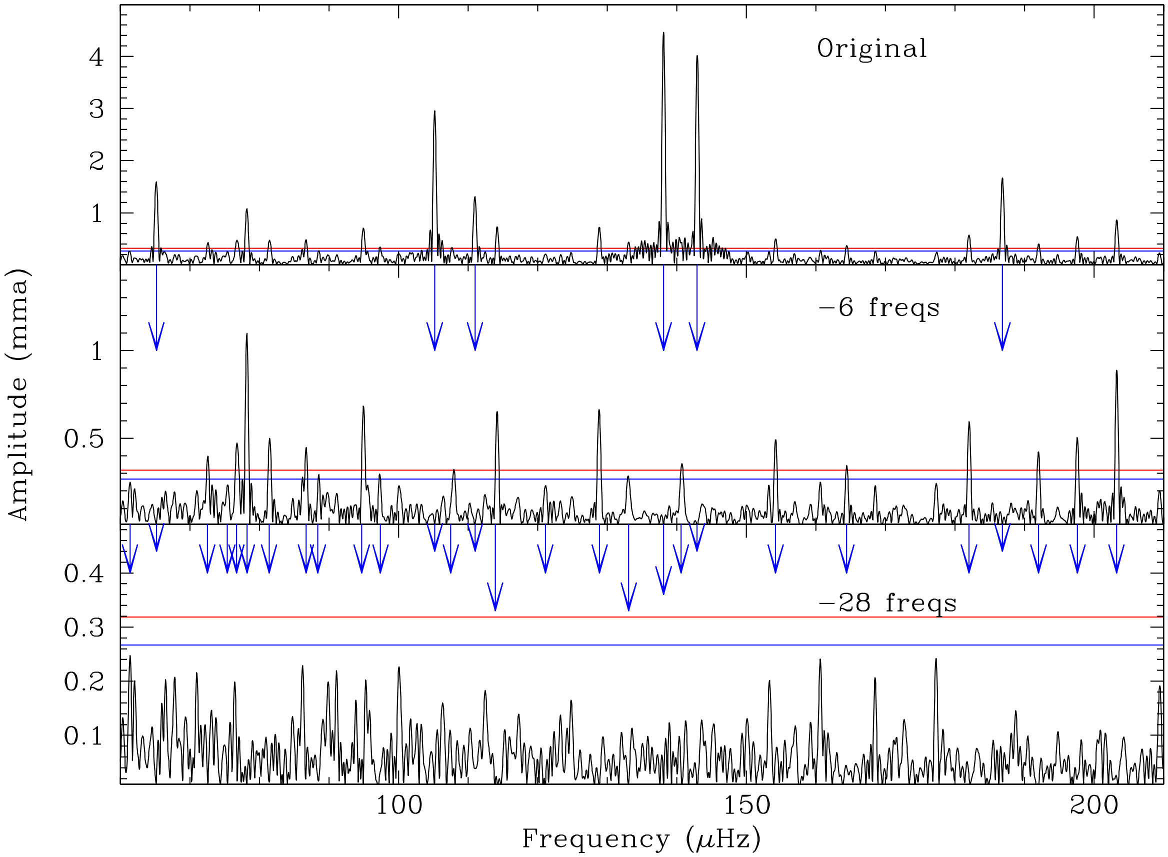

Figure 4. Same as Fig. 3 for KIC010670103. The middle and bottom panels are prewhitened by 6 and 28 frequencies, respectively.

the frequency structure appears in §4.1. As examples of possible complex interactions, f1 is a combination of three different frequency differences, the most obvious of which are differences involving high-amplitude peaks: f19-f5 and f21-f7, but it is also a combination of f24-f16. f2 is a complex combination with some high-amplitude peaks (f19-f3, f21-f7) and some lower-amplitude ones (f20-f4, f25-f16, and f28-f19); although some of these lower-amplitude frequencies are themselves possible combinations of other frequencies. KIC002697388, KIC003527751, and KPD 1943 are marked in a similar way in Tables 3, 4, and 5, though we will not discuss their combinations in the text as we feel these are most likely chance superpositions caused by a high frequency density spanning a large frequency range.

3.2 Hybrid variables

For these stars, the pulsations seem to break into three regions, just as for BA09 (Baran et al. 2009), with periodicities longer than about 40 minutes, typical for $g-$mode pulsators, periodicities shorter

Table 2. Frequencies, periods, amplitudes, and S/N for KIC010670103. Possible combination and difference frequencies are marked as ^{C} and ^{D} and a rudimentary fit of the form $P_\ell = P_{\ell o} + n \cdot \Delta P_\ell$ is given in columns 4 and 5 and discussed in §4.1. Column 6 provides the difference between the observed and asymptotic frequencies. Formal least-squares errors are in parentheses.

ID	Frequency (μHz)	Period (s)	ℓ	n	$\Delta\nu$ (μHz)	Amplitude (mma)	S/N σ
f1^D	61.387 (0.050)	16290.060 (13.247)	1	31	0.03	0.246 (0.051)	4.2
f2^D	65.173 (0.008)	15343.676 (1.790)	-	-	-	1.614 (0.051)	27.2
f3	72.571 (0.031)	13779.639 (5.790)	1	21	0.04	0.409 (0.051)	6.9
f4	75.399 (0.051)	13262.826 (8.883)	1	19	0.12	0.251 (0.052)	4.2
f5	76.807 (0.030)	13019.718 (5.072)	1	18	0.08	0.423 (0.051)	7.1
f6	78.197 (0.012)	12788.238 (1.970)	1	17	0.04	1.063 (0.051)	17.9
f7	81.445 (0.030)	12278.230 (4.476)	1	15	0.01	0.425 (0.051)	7.2
f8	86.702 (0.029)	11533.722 (3.872)	1	12	0.06	0.426 (0.051)	7.2
f9	88.368 (0.048)	11316.349 (6.162)	1	11	0.32	0.258 (0.051)	4.4
f10	94.942 (0.019)	10532.747 (2.096)	1	8	0.10	0.661 (0.051)	11.2
f11	97.361 (0.042)	10271.031 (4.400)	1	7	0.01	0.298 (0.051)	5.0
f12	105.195 (0.004)	9506.147 (0.380)	1	4	0.12	2.984 (0.051)	50.4
f13	107.924 (0.035)	9265.798 (3.012)	1	3	0.01	0.362 (0.051)	6.1
f14	110.956 (0.010)	9012.574 (0.823)	1	2	0.03	1.255 (0.051)	21.2
f15	114.171 (0.019)	8758.812 (1.433)	1	1	0.06	0.672 (0.051)	11.3
f16	121.073 (0.044)	8259.471 (3.007)	1	-1	0.02	0.247 (0.045)	4.2
f17	128.838 (0.016)	7761.695 (0.973)	1	-3	0.05	0.678 (0.045)	11.4
f18	133.053 (0.037)	7515.790 (2.062)	1	-4	0.15	0.300 (0.045)	5.1
f19	138.099 (0.002)	7241.182 (0.130)	2	16	0.10	4.456 (0.046)	75.2
f20	140.711 (0.030)	7106.778 (1.498)	2	15	0.12	0.375 (0.046)	6.3
f21	142.938 (0.003)	6996.041 (0.133)	1	-6	0.19	4.063 (0.045)	68.6
f22^C	154.211 (0.022)	6484.639 (0.925)	1	-8	0.43	0.508 (0.047)	8.6
f23^C	164.421 (0.030)	6081.943 (1.092)	2	8	0.01	0.379 (0.047)	6.4
f24^C	182.038 (0.019)	5493.347 (0.575)	2	4	0.19	0.588 (0.047)	9.9
f25^C	186.807 (0.007)	5353.106 (0.192)	2	3	0.02	1.675 (0.047)	28.3
f26^C	191.993 (0.026)	5208.532 (0.701)	2	2	0.02	0.433 (0.047)	7.3
f27^C	197.565 (0.022)	5061.637 (0.563)	2	1	0.03	0.509 (0.047)	8.6
f28^C	203.248 (0.013)	4920.108 (0.314)	2	0	0.13	0.863 (0.047)	14.6

than five minutes, typical of $p-$mode pulsators, and then a group that are in between with periods ranging from 15 to 30 minutes.

3.2.1 *KIC002697388*

In total, we detected 37 long-period pulsations leaving four regions with unresolved frequencies in KIC002697388 ($K_p = 15.39$, $T_{\rm eff} \approx 23\,900 \pm 300\,$K, $\log g = 5.32 \pm 0.03$; Paper I). These are listed in Table 3 along with their amplitudes and periods and indicated in Fig. 5 with arrows. Unresolved power remains in the FT above the detection limit, which could not be NLLS fitted and the most obvious of these are indicated by longer (red) arrows. Figure 6 is an enlarged view of the low-frequency region.

We also detected a high-frequency peak above the 4σ limit that was not an artefact caused by long-cadence readout. The peak is low amplitude but a 5.4σ detection in the combined data which is significant above the noise. The hybrids are discussed further in §4.3 and until KIC002697388 receives further observations (Q5), we consider it as a candidate hybrid pulsator.

As observed for BA09 (Baran et al. 2009), several of the intermediate frequencies are possible

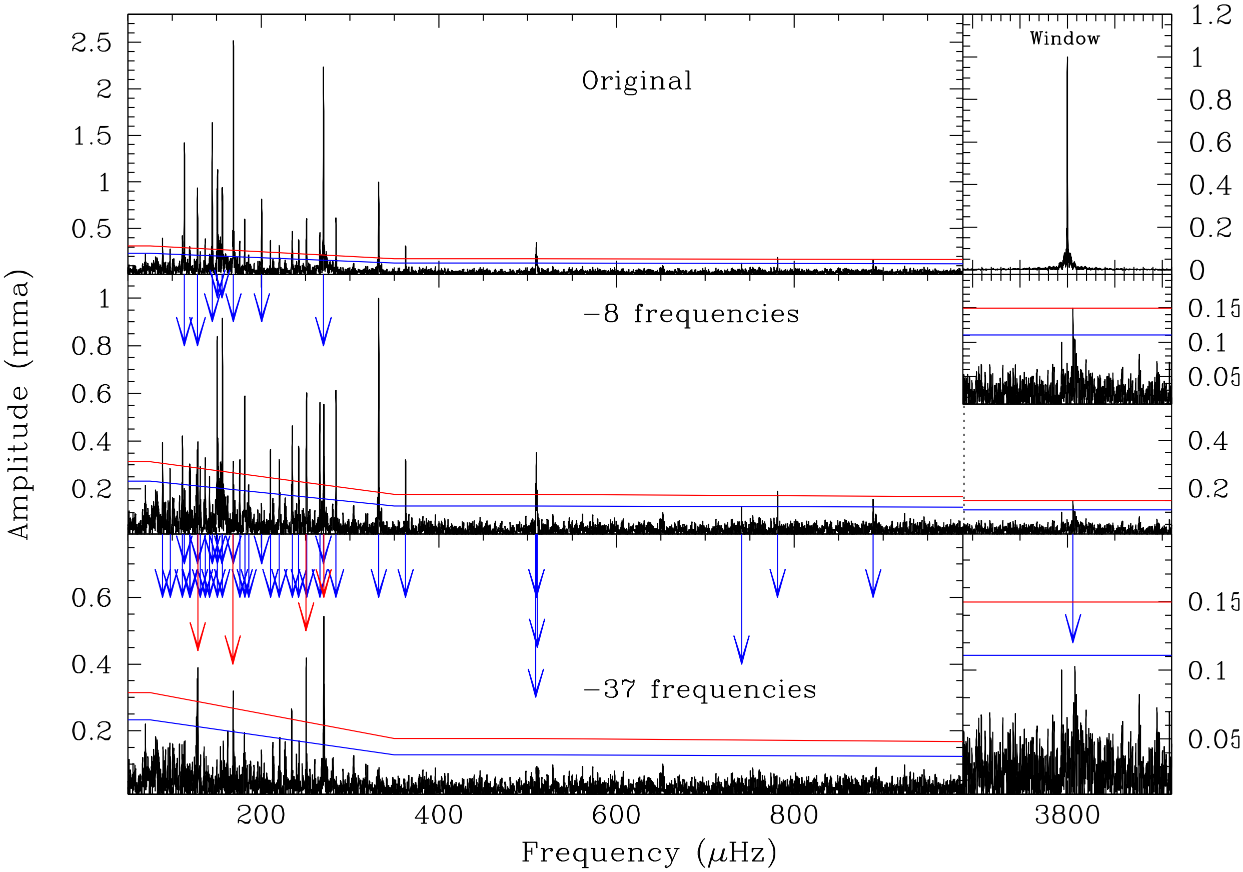

Figure 5. Same as Fig. 3 for KIC002697388. The middle panel has eight frequencies removed and the bottom panel is prewhitened by 37 frequencies. Red arrows indicate likely frequencies that were not fitted (see Fig. 6 for an enlarged view). Note that the vertical scale changes with each panel. The right panels show the window function on top, the middle panel is broken into two sub-panels so the high-frequency regime can be plotted on the same vertical scale as the left panel (separated by a dashed blue line) and an enlarged view better shows the peak in the original FT. The bottom panel is the prewhitened FT.

combination frequencies. As this frequency region is less densely populated in models, it is likely some of these are real combinations. However, not all of the frequencies in this range can be attributed to combination frequencies.

3.2.2 KIC003527751

All of the pulsation amplitudes of KIC003527751 ($K_p = 14.86$, $T_{\rm eff} \approx 27\,900 \pm 200\,$K, $\log g = 5.37 \pm 0.09$; Paper I) are quite low and would almost certainly be missed in ground-based observations, yet they are easily detected in these *Kepler* data. In total, we detected 41 pulsation frequencies with no residuals above the detection limit. These are listed in Table 4 along with their amplitudes and periods and indicated in Fig. 7 with arrows.

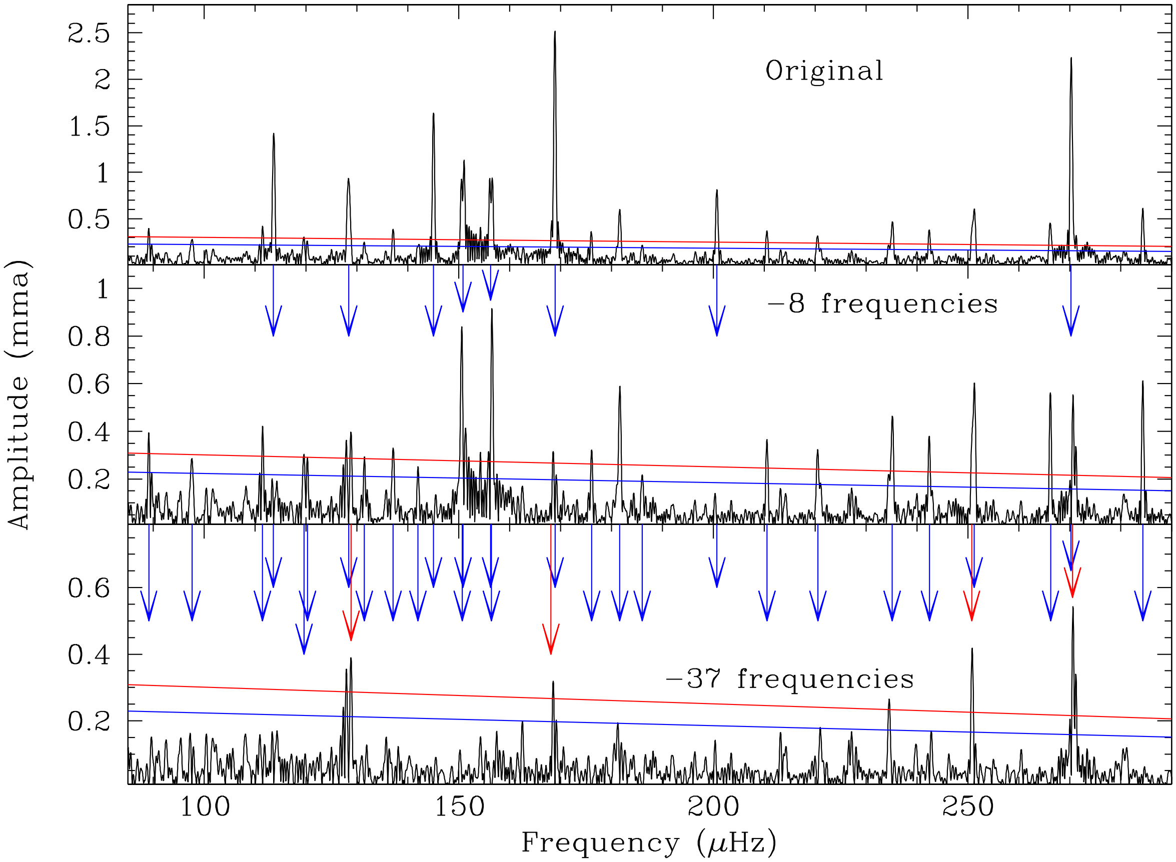

Figure 6. Temporal spectrum of KIC002697388 between 100 and 300 μHz. Note that the vertical scale changes with each panel.

3.2.3 KPD 1943 (KIC005807616)

In total, we detected 21 frequencies with confidence, four frequencies that were marginally below the detection limit, and still there remained three regions of unresolved power for KPD 1943 ($K_p = 15.02$, $T_{\rm eff} \approx 27\,100 \pm 200\,$K, $\log g = 5.51 \pm 0.02$; Paper I). These are listed in Table 5 along with their amplitudes and periods and indicated in Fig. 8 with blue and magenta arrows, respectively. We note that an independent analysis in Paper IV obtained a slightly different, but generally consistent, set of frequencies.

Figure 9 shows the unresolved regions, with red arrows indicating the frequencies listed in Table 5.

4 DISCUSSION

The V1093 Her pulsators all have periods longer then an hour and the extremes scale roughly with $\log g$ and $T_{\rm eff}$. KIC010670103 is the coolest sdBV detected to date and has the longest periods, reaching nearly 4.5 h in duration. Such long periods would obviously be very difficult to detect

Table 3. Frequencies, periods, amplitudes, and S/N for KIC002697388 Formal least-squares errors are in parentheses. ^{C} and ^{D} indicates possible combination and difference frequencies. Unresolved frequencies which could not be NLLS fitted are listed at the bottom with amplitudes estimated directly from the FT.

ID	Frequency (μHz)	Period (s)	Amplitude (mma)	S/N
f1^D	89.109 (0.017)	11222.207 (2.079)	0.385 (0.026)	6.8
f2	97.579 (0.023)	10248.154 (2.432)	0.274 (0.026)	4.9
f3	111.477 (0.015)	8970.500 (1.205)	0.426 (0.026)	7.8
f4^D	113.649 (0.006)	8799.008 (0.459)	1.441 (0.036)	26.5
f5	119.504 (0.024)	8367.893 (1.699)	0.272 (0.027)	5.0
f6	120.305 (0.027)	8312.182 (1.867)	0.244 (0.027)	4.5
f7	128.350 (0.009)	7791.189 (0.548)	0.945 (0.036)	17.8
f8	131.442 (0.022)	7607.932 (1.267)	0.291 (0.026)	5.5
f9	137.085 (0.020)	7294.763 (1.058)	0.320 (0.026)	6.1
f10	141.972 (0.028)	7043.651 (1.375)	0.229 (0.026)	4.4
f11	145.026 (0.005)	6895.323 (0.253)	1.609 (0.036)	31.2
f12	150.670 (0.027)	6637.021 (1.178)	1.371 (0.259)	26.9
f13	150.891 (0.025)	6627.321 (1.090)	1.480 (0.259)	29.0
f14	156.278 (0.044)	6398.864 (1.813)	2.557 (1.765)	50.7
f15	156.397 (0.044)	6393.989 (1.813)	2.553 (1.765)	50.6
f16	168.861 (0.003)	5922.022 (0.118)	2.529 (0.036)	51.3
f17^D	176.073 (0.019)	5679.474 (0.601)	0.336 (0.026)	6.9
f18^D	181.607 (0.011)	5506.391 (0.323)	0.591 (0.026)	12.3
f19	186.048 (0.027)	5374.965 (0.769)	0.236 (0.026)	4.9
f20	200.679 (0.010)	4983.073 (0.257)	0.825 (0.036)	17.8
f21	210.502 (0.017)	4750.550 (0.387)	0.365 (0.026)	8.0
f22	220.453 (0.020)	4536.116 (0.407)	0.317 (0.026)	7.1
f23	235.124 (0.014)	4253.082 (0.250)	0.453 (0.026)	10.5
f24	242.388 (0.016)	4125.623 (0.268)	0.398 (0.026)	9.4
f25	251.250 (0.010)	3980.103 (0.163)	0.609 (0.026)	14.6
f26	266.151 (0.011)	3757.261 (0.160)	0.553 (0.026)	13.7
f27	270.254 (0.004)	3700.224 (0.052)	2.230 (0.036)	55.8
f28^C	284.316 (0.010)	3517.219 (0.128)	0.606 (0.026)	15.7
f29	332.366 (0.006)	3008.732 (0.054)	1.000 (0.025)	29.2
f30^C	362.698 (0.019)	2757.118 (0.141)	0.323 (0.025)	10.1
f31^C	509.169 (0.039)	1963.985 (0.149)	0.165 (0.026)	5.2
f32^C	509.947 (0.019)	1960.990 (0.074)	0.352 (0.027)	11.0
f33^C	510.668 (0.031)	1958.219 (0.120)	0.212 (0.026)	6.6
f34^C	740.877 (0.047)	1349.752 (0.086)	0.126 (0.025)	4.0
f35^C	781.382 (0.031)	1279.784 (0.051)	0.192 (0.025)	6.0
f36	888.917 (0.038)	1124.964 (0.048)	0.157 (0.025)	4.9
f37	3805.906 (0.040)	262.750 (0.003)	0.147 (0.024)	5.3
		Unresolved frequencies		
u38	128.8		0.39	
u39	168.1		0.32	
u40	250.7		0.42	
u41^C	270.5		0.55	

from Earth with interrupting diurnal cycles. KIC007664467 has the fewest frequencies detected in this sample and they are easily resolved. However, this is likely based on the detection limit, so with more data, we will likely find more frequencies. KIC010670103 is the richest V1093 Her pulsator known to date with 28 frequencies.

The hybrid pulsators discovered by *Kepler* are also extremely rich pulsators with over 100 frequencies detected between the three stars. The $p-$mode pulsations were a surprise discovery. While two of the hybrids have temperatures and gravities similar to non-*Kepler* hybrids, we did not

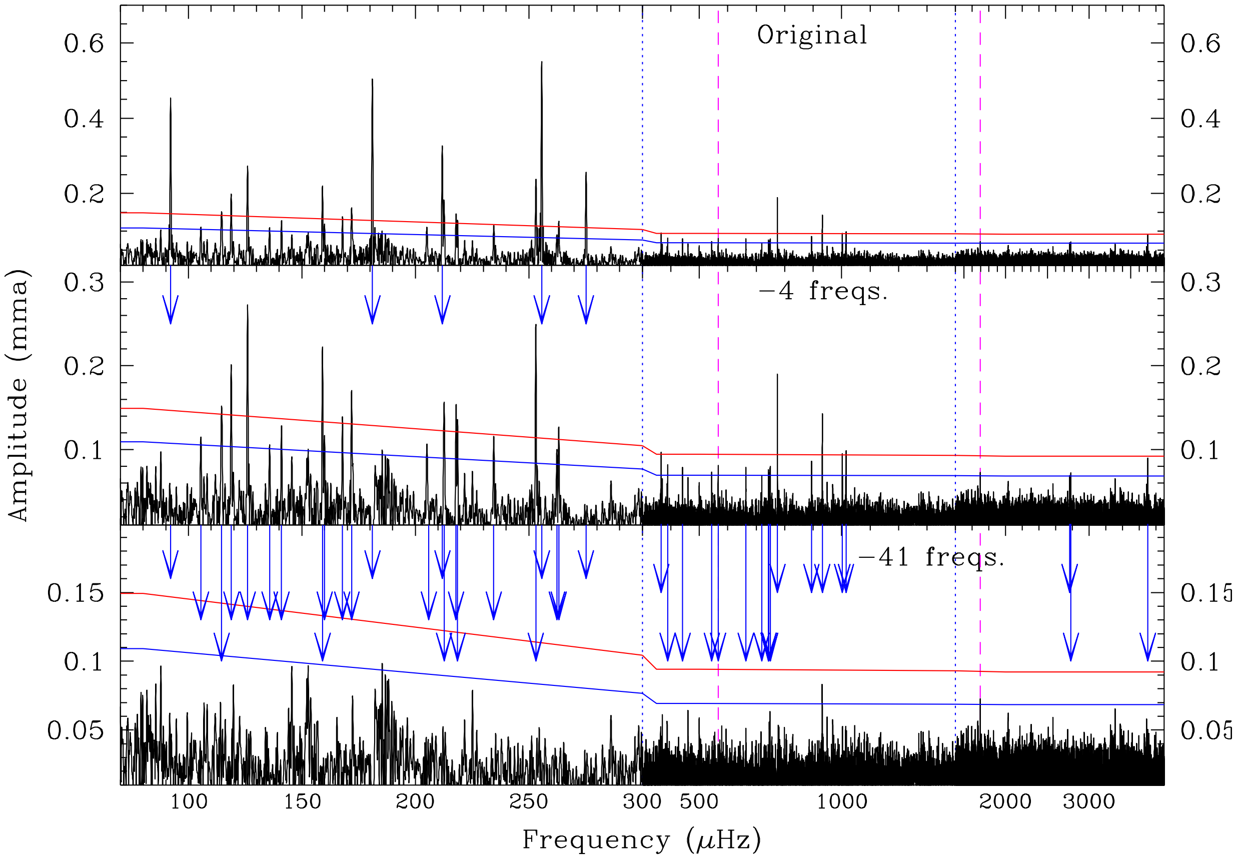

Figure 7. Same as Fig. 3 for KIC003527751. The frequency axis is continuous across the figure, but changes scale at the dotted vertical lines. The top panel shows the original spectrum with subsequent panels prewhitened by four and 41 frequencies. The top right panel shows the window function for these data. Note that the vertical scale changes with each panel.

anticipate hybrids where the $p-$mode amplitudes were smaller than the $g-$mode ones. Similarly, the candidate hybrid KIC002697388 is surprisingly cool. Should subsequent *Kepler* observations (during Q5) confirm the hybrid nature of KIC002697388, it would indeed represent an intriguing object. Driving $p-$mode pulsations at those temperatures is not a problem, but rather depends on the amount of iron enhancement (see Fig. 2 of Charpinet et al. 2007). Defining the extent of the $p-$mode instability region constrains the minimum amount of Z-bump enhancement in the driving region.

4.1 Mode identifications using asymptotic relations

While the crowded $g-$mode frequency density may appear as a disadvantage for model fitting, because we have reached a region where asymptotic relationships may apply, it could prove useful for mode identifications. In turn, observational correlations between modes and frequencies can provide strong model constraints (e.g., Winget et al. 1991).

Table 4. Frequencies, periods, amplitudes, and S/N for KIC003527751. Possible combination and difference frequencies are noted with ^{C} and ^{D} in column 1. Formal least-squares errors are in parentheses.

ID	Frequency (μHz)	Period (s)	Amplitude (mma)	S/N σ
f1	92.144 (0.008)	10852.611 (0.962)	0.455 (0.016)	17.0
f2	105.478 (0.030)	9480.648 (2.717)	0.116 (0.015)	4.4
f3	114.625 (0.023)	8724.069 (1.752)	0.153 (0.015)	6.0
f4	118.825 (0.017)	8415.768 (1.207)	0.207 (0.015)	8.1
f5	126.070 (0.013)	7932.131 (0.821)	0.269 (0.015)	10.7
f6	135.767 (0.034)	7365.565 (1.833)	0.104 (0.015)	4.2
f7^D	141.016 (0.027)	7091.397 (1.380)	0.128 (0.015)	5.2
f8	159.098 (0.016)	6285.436 (0.615)	0.233 (0.015)	9.8
f9	159.878 (0.028)	6254.758 (1.080)	0.132 (0.015)	5.6
f10	167.871 (0.024)	5956.947 (0.845)	0.147 (0.015)	6.3
f11	171.928 (0.020)	5816.402 (0.675)	0.176 (0.015)	7.6
f12	181.052 (0.007)	5523.277 (0.225)	0.503 (0.016)	22.2
f13	205.104 (0.031)	4875.586 (0.743)	0.112 (0.015)	5.2
f14	211.872 (0.011)	4719.823 (0.251)	0.332 (0.016)	15.6
f15	212.672 (0.022)	4702.076 (0.489)	0.158 (0.015)	7.4
f16^D	217.937 (0.026)	4588.472 (0.557)	0.145 (0.016)	6.9
f17^D	218.584 (0.031)	4574.895 (0.649)	0.124 (0.016)	5.9
f18^D	234.546 (0.031)	4263.556 (0.569)	0.119 (0.016)	5.9
f19	253.095 (0.015)	3951.085 (0.230)	0.257 (0.016)	13.2
f20	255.694 (0.007)	3910.932 (0.103)	0.562 (0.016)	29.1
f21^C	262.376 (0.041)	3811.326 (0.596)	0.094 (0.016)	4.9
f22	263.181 (0.030)	3799.665 (0.436)	0.128 (0.016)	6.7
f23	275.216 (0.015)	3633.516 (0.196)	0.251 (0.016)	13.6
f24^C	366.437 (0.035)	2728.982 (0.264)	0.097 (0.014)	5.7
f25^C	388.851 (0.042)	2571.681 (0.278)	0.081 (0.014)	4.7
f26^C	441.541 (0.043)	2264.793 (0.222)	0.079 (0.014)	4.6
f27^C	543.979 (0.048)	1838.307 (0.163)	0.071 (0.014)	4.1
f28	566.404 (0.043)	1765.523 (0.133)	0.080 (0.014)	4.7
f29^C	663.714 (0.044)	1506.672 (0.099)	0.078 (0.014)	4.6
f30	719.535 (0.049)	1389.787 (0.095)	0.069 (0.014)	4.0
f31	743.649 (0.098)	1344.720 (0.177)	0.098 (0.049)	5.7
f32	743.918 (0.105)	1344.234 (0.189)	0.091 (0.049)	5.3
f33^C	749.222 (0.042)	1334.717 (0.075)	0.081 (0.014)	4.7
f34	774.700 (0.018)	1290.822 (0.030)	0.190 (0.014)	11.1
f35	894.390 (0.039)	1118.081 (0.049)	0.087 (0.014)	5.1
f36^C	932.440 (0.024)	1072.455 (0.028)	0.141 (0.014)	8.2
f37^C	1002.470 (0.036)	997.536 (0.036)	0.095 (0.014)	5.5
f38^C	1015.819 (0.035)	984.427 (0.034)	0.098 (0.014)	5.7
f39	2767.427 (0.050)	361.346 (0.007)	0.068 (0.014)	4.0
f40	2782.505 (0.048)	359.388 (0.006)	0.071 (0.014)	4.1
f41	3703.293 (0.038)	270.030 (0.003)	0.089 (0.014)	5.2

In the asymptotic limit for $n \gg \ell$, $g-$modes should be equally spaced in period for consecutive values of n (Smeyers & Tassoul 1987), where n represents the number of radial nodes and ℓ is the number of surface nodes. This asymptotic behaviour has been observed very clearly in pulsating white dwarfs (e.g. Kawaler & Bradley 1994). The relationship is

$$\Pi_{n,\ell} = n \times \frac{\Pi_o}{\sqrt{\ell\,(\ell+1)}}$$

and indicates a second important feature which is useful for mode identifications. Modes of consecutively higher degree ℓ will be spaced closer together in a predictable relation and modes of the same n but differing ℓ will be related in period. In particular, the relations between $\ell = 1$ and 2

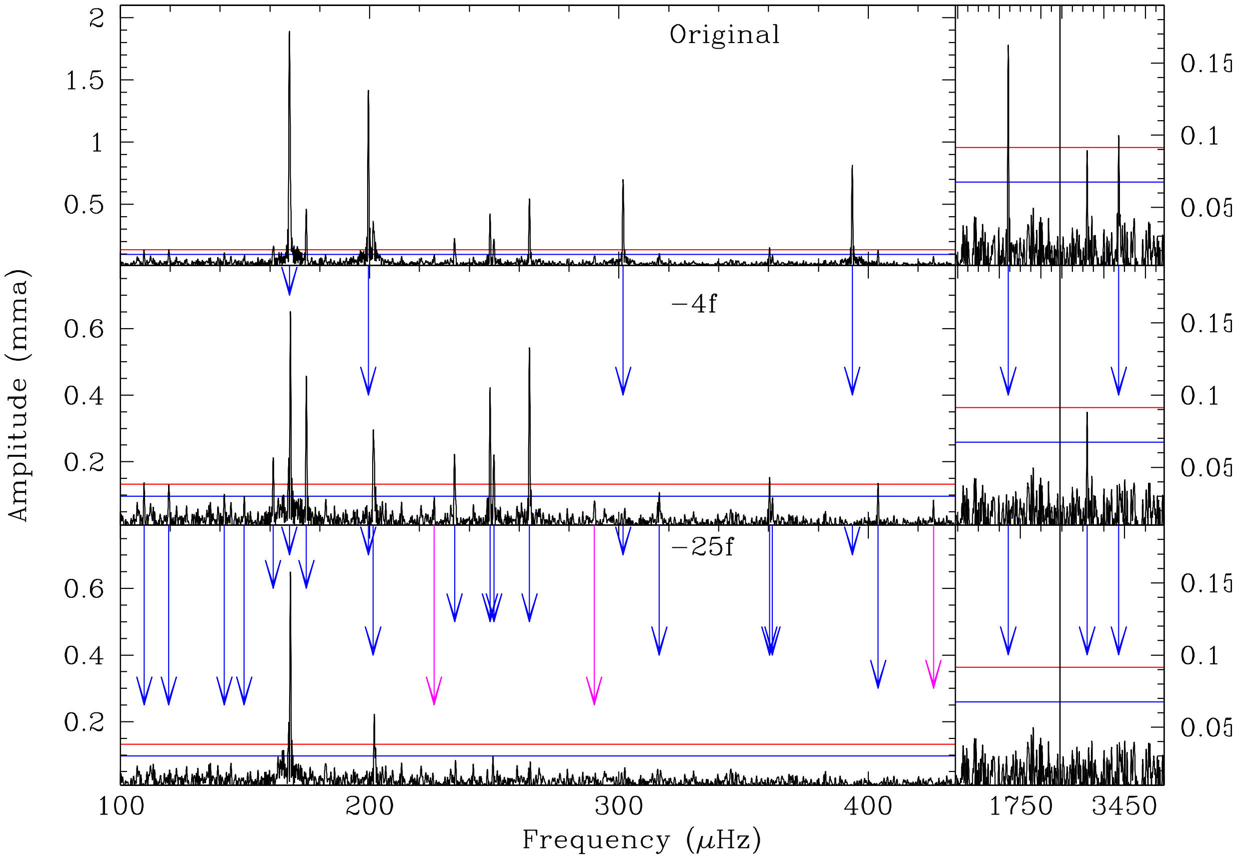

Figure 8. Same as Fig. 3 for KPD 1943. The middle panel is prewhitened by 4 frequencies and the bottom is panel is prewhitened by 25 frequencies. Unresolved regions are shown in Fig. 9.

modes for period spacings and related overtones will be $\sqrt{3}$. Specifically,

$$\Delta\Pi_{\ell=2} = \frac{\Delta\Pi_{\ell=1}}{\sqrt{3}} \quad \text{and} \quad \Pi_{n,\ell=2} = \frac{\Pi_{n,\ell=1}}{\sqrt{3}}$$

for large n.

A quick examination of KIC010670103's periods easily shows that there are common period spacings. As such, we used it as a test to see how thoroughly asymptotic relations could apply. Additionally, KIC010670103 has lots of periods to work with, but not so many as to make the task daunting. As we do not observe frequency multiplets, we assume that rotational splitting can be neglected. KIC010670103 shows several spacings around 145 and 250 s and we also noticed that the 145 s spacings mostly occurred for shorter periods (higher frequencies) and the 250 s spacings for longer periods, as would be expected. Upon closer examination, it is obvious that $145 \approx 250/\sqrt{3}$ and that several pairs of periods are also related directly by $1/\sqrt{3}$. This prompted one of us (sdk) to produce fits to the periods for each spacing of the form $P_\ell = P_{\ell o} + n \cdot \Delta P_\ell$. For the apparent $\ell = 1$ modes, the fit is $P_1 = 8512.08 + n \cdot 251.16$ and for the $\ell = 2$ modes it is $P_2 = 4916.58 + n \cdot 145.59$. The base frequencies were chosen such that the shortest period

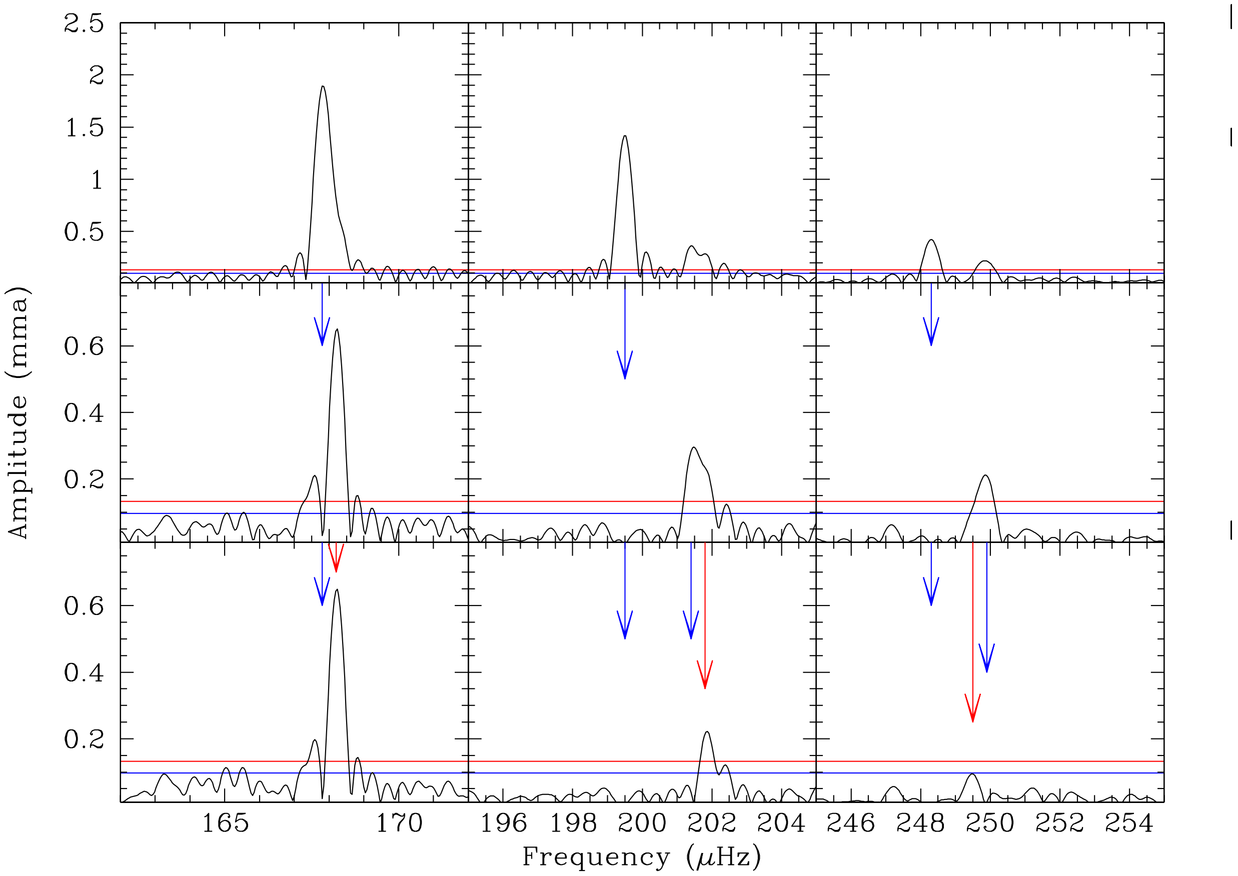

Figure 9. Temporal spectra for KPD 1943 showing unresolved regions. Each panel is 10μHz wide and blue arrows indicate prewhitened frequencies while red ones indicate unresolved frequencies listed in Table 5.

in KIC010670103 is $n = 0$ and the associated $\ell = 1$ period would have the same n value. This scheme produces some negative n values for the $\ell = 1$ sequence, but it is very important to note that while consecutive n values represent consecutive overtones within the star, the values themselves are not representative of the actual n value for any given period. Indeed, they must *not* be associated with the actual value, or asymptotic relations would not apply.

We tested the sequence of period spacings using Komogorov-Smirnov statistical tests (Kawaler 1988) and inverse variance tests (O'Donoghue 1994), along with Monte Carlo simulations using randomly selected periods within the observed range. The observed sequence is statistically significant at the 99.99% level based on these tests. The results of these fits are shown in columns 4, 5, and 6 of Table 2 where the difference between the asymptotic relation period and the observed period (column 6) is given in frequency, so it can be compared with the $1/T$ resolution of $0.43\,\mu$Hz. Amazingly, these two relations fit 27 of the 28 periodicities observed in KIC010670103, with f24 fitting at the $1/T$ resolution limit. Additionally, there are several pairs of frequencies that are related overtones (same n value). This provides very powerful evidence that nearly all of the

Table 5. Frequencies, periods, amplitudes, and S/N for KPD 1943. Formal least-squares errors are in parentheses. Possible combination and difference frequencies are marked in column 1 with ^{C} and ^{D}.

ID	Frequency (μHz)	Period (s)	Amplitude (mma)	S/N S/N
f1^D	109.50 (0.04)	9132.311 (2.979)	0.14 (0.02)	5.8
f2	119.44 (0.04)	8372.266 (2.611)	0.13 (0.02)	5.4
f3	141.73 (0.03)	7055.779 (1.667)	0.10 (0.01)	4.1
f4	149.73 (0.05)	6678.527 (2.251)	0.10 (0.02)	4.1
f5^D	161.32 (0.02)	6198.841 (0.892)	0.21 (0.02)	8.7
f6	167.82 (0.00)	5958.808 (0.092)	1.90 (0.02)	78.4
f7	174.64 (0.01)	5726.085 (0.353)	0.46 (0.02)	19.0
f8	199.50 (0.00)	5012.561 (0.088)	1.41 (0.02)	58.2
f9	201.49 (0.02)	4963.086 (0.410)	0.30 (0.02)	12.4
f10	234.06 (0.02)	4272.329 (0.407)	0.22 (0.02)	9.1
f11	248.30 (0.01)	4027.352 (0.191)	0.42 (0.02)	17.3
f12	249.87 (0.02)	4002.153 (0.374)	0.21 (0.02)	8.7
f13	264.11 (0.01)	3786.345 (0.130)	0.54 (0.02)	22.3
f14	301.67 (0.01)	3314.876 (0.078)	0.69 (0.02)	28.5
f15^C	316.18 (0.05)	3162.719 (0.463)	0.11 (0.02)	4.5
f16	360.44 (0.03)	2774.381 (0.258)	0.15 (0.02)	6.2
f17	393.61 (0.01)	2540.590 (0.039)	0.82 (0.02)	33.8
f18	403.96 (0.04)	2475.513 (0.222)	0.13 (0.02)	5.4
f19	1744.29 (0.02)	573.300 (0.007)	0.16 (0.01)	9.5
f20	3432.08 (0.04)	291.369 (0.003)	0.09 (0.01)	5.3
f21	3447.23 (0.04)	290.088 (0.003)	0.10 (0.01)	5.9
	Suggested Frequencies			
s22^D	225.90 (0.05)	4426.714 (0.964)	0.10 (0.02)	4.1
s23	290.19 (0.06)	3446.011 (0.720)	0.08 (0.02)	3.3
s24	361.63 (0.06)	2765.289 (0.443)	0.09 (0.02)	3.7
s25^C	426.18 (0.06)	2346.420 (0.328)	0.08 (0.02)	3.3
	Unresolved Frequencies			
u26	168.2		0.99	
u27^D	202.4		0.36	
u28	249.5		0.16	

observed periodicities in KIC010670103 are $\ell = 1$ and 2 modes as the two sequences are not independent spacings, but rather include six pairs of periods related by $1/\sqrt{3}$, which means these must be the same n value (whatever that may be) intrinsically to the star.

Further investigations will be warranted once the longer-duration (Q5 and beyond) data sets are obtained, both for KIC010670103 and other $g-$mode pulsators. We also note that a satisfactory model fit has been obtained for KPD 1943 (Paper IV) without the aid of asymptotics (and indeed the model fit indicates the frequencies are far from satisfying the asymptotic behaviour).

4.2 Short-period amplitude stability

As some low-amplitude short-period $p-$mode frequencies can appear transitory (Paper I), we divided our data into four one-week sections, and fixing the frequencies, fitted the phases and amplitudes. As can be seen in Fig. 10, except for KIC002697388, the phases are stable and while their amplitudes waver a bit (some get quite low), nearly all are constant within the 1σ errorbars. However while KPD 1943's f21's phases seem stable, the amplitude continually decreases and the

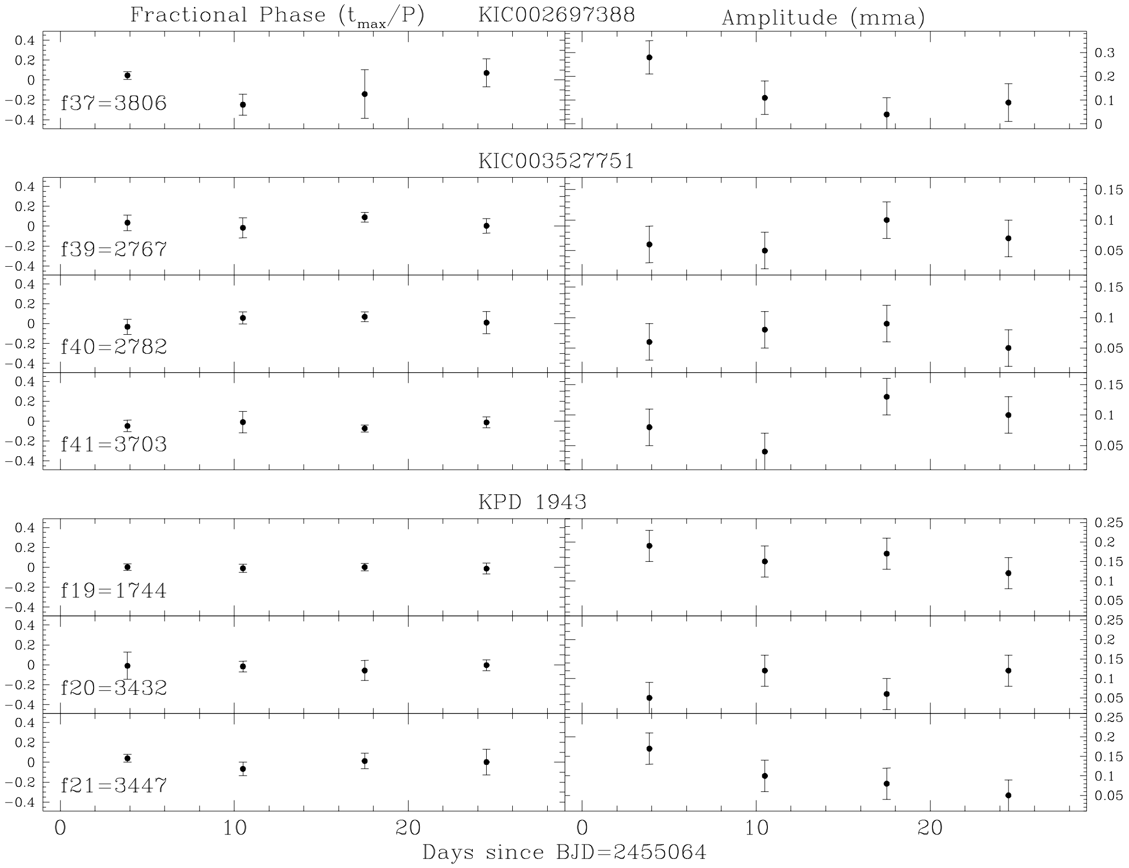

Figure 10. Phases (left panels) and amplitudes (right panels) for the high-frequency variations determined over one week intervals.

last measurement is nearly undetectable. We also note that all three of KPD 1943's short-period $p-$mode frequencies lie within $30\,\mu$Hz of an LC read-time artefact. While we do not think they are related, it is a coincidence that compels further investigation. It will be interesting to see how the high-frequency amplitudes vary, presuming the frequencies persist at detectable levels during *Kepler's* next observational run on these stars. Those data will also be useful for determining relations to the LC artefacts.

4.3 Hybrid amplitudes

Compared to previously known hybrid pulsators, these *Kepler* variables are unusual in that the $g-$mode pulsations have higher amplitudes than the highest $p-$mode ones (or one, for KIC003527751). For comparison with the previously known hybrids in §1, the highest-amplitude $p-$ and $g-$mode pairs for KIC002697388, KIC003527751, and KPD 1930 are $0.15 : 2.56$, $0.09 : 0.56$, and $0.16 : 1.90$ which are reversed from the non-*Kepler* hybrids. While the results are very preliminary and subject to systematics between various spectral line fitting procedures, it appears that the $g-$mode dominated hybrids are very slightly cooler than the $p-$mode dominated ones. If verified this could indicate a real change in how the pulsation power is applied to differing regions of the star as $g-$modes are more sensitive to core conditions while $p-$modes are atmospheric in nature.

5 CONCLUSIONS AND FUTURE WORK

The data presented here confirm the potential of the *Kepler* mission for sdB asteroseismology. We have identified pulsations with amplitudes blending into the detection limit. We anticipate that further, longer-duration observations during *Kepler's* second year of operation will resolve and detect even more, lower-amplitude frequencies and unambiguously determine if the first hybrids with lower $p-$ mode amplitudes have been detected.

Frequency density is not an issue for $g-$mode pulsators (Reed et al. 2004b) as models provide many closely spaced frequencies in this region (Fontaine et al. 2006; Jeffery and Saio 2007; Hu et al. 2009). Yet pulsation models have found it easier to drive high-degree ($\ell \geqslant 3$) modes and since the detected amplitudes continue down to the detection limit, and likely beyond, it is likely that high-degree modes are present. *Kepler* can test this critical model assumption in that with more data and a lower detection threshold, it may be possible to determine if $\ell \geqslant 3$ are truly present. As $\ell \geqslant 3$ have a large degree of geometric cancellation (Charpinet et al. 2005; Reed et al. 2005), if their amplitudes are intrinsically similar to low-degree modes, then their observed amplitudes would be significantly reduced. Sustained *Kepler* photometry will be able to detect such low-amplitude frequencies.

An asymptotic limit approach has been applied to the period spacings of KIC010670103. The results show a good fit to nearly all the observed periodicities, identifying all but one frequency as $\ell = 1$ or 2 modes. Both the spacings and relations between the two sets agree with the expected $1/\sqrt{3}$ asymptotic relations to surprising accuracy. This is remarkable for two reasons: firstly in that it indicates that $\ell = 1$ and 2 modes are not only present, but predominant in at least one star and secondly in that asymptotic relations may be a useful method for correlating periodicities with modes for sdB stars. A future paper will examine the period spacings of all the *Kepler* $g-$mode pulsators and attempt to constrain mode identifications.

We have shown results from a study of the first *Kepler* data on newly-discovered V1093 Her variables. Both stars likely have variations of sufficient amplitude to have been detected from ground-based observations[1], though they are all fainter than 15^{th} magnitude. Yet the majority of pulsation amplitudes we detect are below 0.1%, which is very difficult to detect from the ground, especially taking atmospheric transparency variations into consideration. For comparison, power-weighted mean frequencies were calculated which result in $f_{\rm med}$ =208.0, and 131.6 μHz for KIC007664467, and KIC010670103, respectively. A ground-based observing night (of 8 h) would obtain 6.0, and 3.8 continuous pulsation cycles before having a daytime gap. *Kepler* has obtained over 550, and 352 pulsation cycles of nearly continuous, homogeneously-obtained data. These provide the richest $g-$mode pulsation spectra obtained to date, which are essential for understanding these complex pulsators.

In these stars we detected seven and 28 frequencies, with the possibility that some could be combination frequencies. We have also detected the longest periods (near 4.5 h) known to date, for the coolest known sdBV star ($T_{\rm eff} \approx 20\,900\,$K; Paper I), thus extending the temperature range of pulsators. As periodicities are sensitive to the stellar radius, measured via gravities, the stars with the lowest gravities should have the longest periods. As both stars have similar gravities, their shortest periods are similar, but KIC010670103's cooler nature seems to drive higher overtones (and thus longer periods).

We have examined the first three hybrid subdwarf B pulsators discovered by the *Kepler* mission. These stars are unique among hybrid pulsators for several reasons including the abundance of $g-$mode frequencies, the reversed amplitude ratios between the $p-$ and $g-$modes compared to non-*Kepler* hybrids, the complexities of their combination frequencies, and the extremely low detection limit that *Kepler* has compared to ground-based observations. And yet they have a resemblance to the best-studied hybrid, BA09, in that these stars all have intermediate frequencies, and BA09 also has combination frequencies.

In these stars we detect 37, 41, and 21 frequencies for KIC002697388, KIC003527751, and KPD 1943, respectively. In all cases, combination frequencies may be present and the pulsations were detected right down to the detection limit, indicating that further data will reveal more periodicities. All of these stars show widely distributed frequencies. KIC002697388 and KIC003527751 show "gap" frequencies like BA09, which lie between the $g-$ and $p-$mode regimes.

These stars will certainly be invaluable to discerning the interior structure of sdB stars, as their pulsations span a large range of frequencies, with each frequency, and frequency region likely probing a different layer within the star itself. Such constraints can be useful for determining if differential internal rotation exists as well as probing narrow ionization (and thus convective) zones.

---

[1] With the contamination correction, which we did not apply.

Typically, a key to discerning interior conditions of stars is the association of frequencies with pulsation modes. It is possible that the asymptotic approach, as has been applied to KIC010670103, or possible combination frequencies, as has been done for ZZ Ceti stars (Yeates et al. 2005), may be useful for determining modes. Such constraints could be very useful for distinguishing between various models, modelling methods and help with mismatches between observed and theoretical period distributions.

ACKNOWLEDGMENTS: Funding for this Discovery mission is provided by NASA's Science Mission Directorate. The authors gratefully acknowledge the entire *Kepler* team, whose efforts have made these results possible. ACQ is supported by the Missouri Space Grant Consortium, funded by NASA. The research leading to these results has received funding from the European Research Council under the European Community's Seventh Framework Programme (FP7/2007–2013)/ERC grant agreement n°227224 (PROSPERITY) and from the Research Council of K.U.Leuven (GOA/2008/04). AB gratefully acknowledges support from the Polish Ministry under grant No. 554/MOB/2009/0.

REFERENCES

Baran A., Pigulski A., Koziel D., Ogloza W., Silvotti R., Zola S. 2005, MNRAS, 360, 737

Baran A., et al. 2009, MNRAS, 392, 1092

Baran A., Fox-Machado, L. 2010, Ap&SS, *in press*

Borucki W.J., et al. 2010, Science, 327, 977

Charpinet S., Fontaine G., Brassard P., 1996, ApJ, 471, L103

Charpinet S., Fontaine G., Brassard P., 2001, PASP, 113, 775

Charpinet S., Fontaine G., Brassard P., Green E.M., Chayer P. 2005, A&A, 437, 575

Charpinet S., Fontaine G., Brassard P., Chayer P., Green E. M., Randall S. K., 2007, CoAst, 150, 241

Downes R.A., 1986, ApJS, 61, 569

Fontaine G., Green E. M., Chayer P., Brassard P., Charpinet S., Randall, S.K., 2006, BaltA, 15, 211

Gilliland R.L., et al. 2010a, PASP, 122, 131

Gilliland R.L., et al. 2010b, ArXiv e-prints

Green E. M., et al. 2003, ApJ, 583, L31

Heber, U. 1984, A&A, 130, 119

Heber U., 2009, A&A Annual Reviews, 47, 211

Hu et al., 2009 A&A, 508, 869

Jeffery C.S., Saio H., 2007, MNRAS, 378, 379

Kawaler S.D., et al., 2010, MNRAS Paper II

Kawaler S.D., et al., 2010, MNRAS Paper V

Kawaler S.D. 1988, in IAU Symp. 123: Advances in Helio- and Asteroseismology, eds. J. Christensen-Dalsgaard and S. Frandsen, (Dordrecht: Reidel), 329

Kawaler S.D., Bradley P.A., 1994, ApJ, 427, 415

Kazarovets E. V., Samus N. N., Durlevich O. V., Kireeva N. N., Pastukhova E. N., Pojmanski G., 2009, VizieR On-line Data Catalog: J/AZh/86/1088.

Kilkenny D., Koen C., O'Donoghue D., Stobie R.S., 1997, MNRAS, 285, 640

Koch D., et al., 2010, ApJ, 713, 79

Lutz R., Schuh S., Silvotti R., Bernabei S., Dreizler S., Stahn T., Hügelmyer S. D. , 2009, A&A, 496, 469

O'Donoghue, D. 1994, MNRAS, 270, 222

Østensen R., et al., 2010a, A&A, 513, A6

Østensen, R. et al., 2010b, MNRAS submitted, Paper I

Reed M.D. et al., 2004, ApJ, 607 445

Reed M.D., Brondel B.J., Kawaler S.D., 2005, ApJ, 634, 602

Reed M. D., Terndrup D. M., Zhou A.-Y., Unterborn C. T., An D., Eggen J. R., 2007, MNRAS 378, 1049

Saffer, R.A., Bergeron P., Koester D., Liebert J., 1994, ApJ, 432, 351

Schuh S., Huber J., Dreizler S., Heber U., O'Toole S. J., Green E. M., Fontaine G., 2006, A&A, 445, 31

Silvotti R., Handler G., Schuh S., Castanheira B., Kjeldsen, H., 2009, CoAst, 159, 97

Smeyers P., Tassoul M., 1987, ApJ, 65, 429

Van Grootel, V., et al. 2010, ApJ., submitted, Paper IV

Winget D.E., et al. (The Whole Earth Telescope Collaboration), 1991, ApJ, 378, 326

Yanny B., et al. 2009, AJ, 137.4377

Yeates C. M., Clemens J. C., Thompson S. E., Mullally F., 2005, ApJ, 635, 1239